

## Supporting Information

# Non-conjugated Polymer Regulated Photoelectrochemical Water Oxidation

Jiao-Nan Yuan<sup>a</sup>, Xian Yan<sup>a</sup>, Bing-Xiong Zheng<sup>a</sup>, Jia-Qi Chen<sup>a</sup>, Fang-Xing Xiao<sup>a, b\*</sup>

a. College of Materials Science and Engineering, Fuzhou University, New Campus, Minhou, Fujian  
Province, 350108, China.

b. State Key Laboratory of Structural Chemistry, Fujian Institute of Research on the Structure of Matter,  
Chinese Academy of Sciences, Fuzhou, Fujian 350002, PR China.

E-mail: [fx Xiao@fzu.edu.cn](mailto:fx Xiao@fzu.edu.cn)

## Table of Contents

	Page NO.
<b>Experimental section</b> .....	S1
<b>Figure S1.</b> Molecular structure of PAH.....	S4
<b>Figure S2.</b> Zeta potentials of WO <sub>3</sub> NRAs and PAH aqueous solution.....	S5
<b>Figure S3.</b> Schematic illustration of interface configuration between MOs and PAH.....	S6
<b>Figure S4.</b> SEM images of WO <sub>3</sub> NPAs with elemental mapping and EDS results.....	S7
<b>Figure S5.</b> SEM images of WO <sub>3</sub> -(PAH) <sub>4</sub> with elemental mapping and EDS results.....	S8
<b>Figure S6.</b> SEM images of WO <sub>3</sub> -(PAH) <sub>4</sub> -calcined with elemental mapping and EDS results.....	S9
<b>Figure S7.</b> TEM and HRTEM images of WO <sub>3</sub> NPAs.....	S10
<b>Figure S8.</b> FTIR spectra of WO <sub>3</sub> -(PAH) <sub>n</sub> (n = 1, 2, 4, 6).....	S11
<b>Figure S9.</b> Locally magnified Raman spectra of WO <sub>3</sub> , WO <sub>3</sub> -(PAH) <sub>4</sub> and WO <sub>3</sub> -(PAH) <sub>4</sub> -calcined.....	S12
<b>Figure S10.</b> Survey spectra of WO <sub>3</sub> -(PAH) <sub>4</sub> , WO <sub>3</sub> NPAs & WO <sub>3</sub> -(PAH) <sub>4</sub> -calcined, and high-resolution C 1s spectrum of WO <sub>3</sub> -(PAH) <sub>4</sub> .....	S13
<b>Figure S11.</b> LSV results and I-t responses of WO <sub>3</sub> and WO <sub>3</sub> -(PAH) <sub>n</sub> (n = 1, 2, 4, 6).....	S14
<b>Figure S12.</b> LSV results and I-t responses of WO <sub>3</sub> and WO <sub>3</sub> -(PAH) <sub>4</sub> -X (X=150, 250, 350, 450 °C).....	S15
<b>Figure S13.</b> TGA curve of WO <sub>3</sub> -(PAH) <sub>4</sub> heterostructure.....	S16
<b>Figure S14.</b> UV-vis absorption spectrum of PAH aqueous solution.....	S17
<b>Figure S15.</b> LSV results of WO <sub>3</sub> -(PAH) <sub>4</sub> and WO <sub>3</sub> NPAs in Na <sub>2</sub> SO <sub>4</sub> aqueous solution with (solid line) and without (dash line) adding Na <sub>2</sub> SO <sub>3</sub> .....	S18
<b>Figure S16.</b> CV curves of PAH.....	S19
<b>Figure S17.</b> Mott-Schottky plots of WO <sub>3</sub> -(PAH) <sub>4</sub> and WO <sub>3</sub> .....	S20
<b>Figure S18.</b> After reaction XRD results, XPS results and TEM and HRTEM images for WO <sub>3</sub> -(PAH) <sub>4</sub> .....	S21
<b>Figure S19.</b> In-situ irradiated high-resolution XPS spectra of Cl 2p for WO <sub>3</sub> -(PAH) <sub>4</sub> .....	S22
<b>Figure S20.</b> SEM images of photodeposited PbO <sub>2</sub> with elemental mapping results.....	S23
<b>Figure S21.</b> SEM images of photodeposited Cr <sub>2</sub> O <sub>3</sub> with elemental mapping results.....	S24
<b>Figure S22.</b> High-resolution Pb 4f spectra of PbO <sub>2</sub> and Cr 2p spectra of Cr <sub>2</sub> O <sub>3</sub> .....	S25
<b>Figure S23.</b> SEM images of TiO <sub>2</sub> NRAs and TiO <sub>2</sub> -(PAH) <sub>4</sub> .....	S26
<b>Figure S24.</b> SEM images of ZnO NRAs and ZnO-(PAH) <sub>4</sub> .....	S27
<b>Figure S25.</b> XRD patterns and FTIR spectra of TiO <sub>2</sub> NRAs & TiO <sub>2</sub> -(PAH) <sub>4</sub> , ZnO NRAs & ZnO-(PAH) <sub>4</sub> .....	S28

<b>Figure S26.</b> PL spectra of TiO <sub>2</sub> NRAs & TiO <sub>2</sub> -(PAH) <sub>4</sub> and ZnO NRAs & ZnO-(PAH) <sub>4</sub> .....	S29
<b>Figure S27.</b> PEC performances of corresponding TiO <sub>2</sub> -based photoanodes.....	S30
<b>Figure S28.</b> PEC performances of corresponding ZnO-based photoanodes.....	S31
<b>Figure S29.</b> M-S results and DRS results of WO <sub>3</sub> , TiO <sub>2</sub> and ZnO at 1000 Hz.....	S32
<b>Table S1.</b> Peak position with corresponding functional groups for photoanodes.....	S33
<b>Table S2.</b> Chemical bond species vs. B.E. for different photoelectrodes.....	S34
<b>Table S3.</b> Fitted EIS results of prepared WO <sub>3</sub> -based photoanodes under simulated solar light irradiation..	S35
<b>Table S4.</b> Fitted EIS results of prepared WO <sub>3</sub> -based photoanodes under visible light irradiation.....	S36
<b>Reference</b> .....	S37

## Experimental Section

### 1. Materials

Fluorine-doped tin oxide glass (FTO, 50 mm × 10 mm × 20 mm, 99.9%), deionized water (DI H<sub>2</sub>O, Millipore, 18.2 MΩ·cm resistivity), sodium tungsten dihydrate (Na<sub>2</sub>WO<sub>4</sub>·2H<sub>2</sub>O), hydrochloric acid (HCl), ammonium oxalate ((NH<sub>4</sub>)<sub>2</sub>C<sub>2</sub>O<sub>4</sub>), poly (allylamine hydrochloride) (PAH, average Mw=17.5 kDa), sodium chloride (NaCl), titanium butoxide (C<sub>16</sub>H<sub>36</sub>O<sub>4</sub>Ti), Zinc acetate dihydrate (Zn(CH<sub>3</sub>COO)<sub>2</sub>·2H<sub>2</sub>O), ethanolamine (C<sub>2</sub>H<sub>7</sub>NO), zinc nitrate hexahydrate (Zn(NO<sub>3</sub>)<sub>2</sub>·6H<sub>2</sub>O), methenamine ((CH<sub>2</sub>)<sub>6</sub>N<sub>4</sub>), Sodium sulfate (Na<sub>2</sub>SO<sub>4</sub>) were obtained from Sigma-Aldrich. All the materials above were used directly without further purification.

### 2. Preparation of WO<sub>3</sub> nanoplate arrays (NPAs) substrate

0.231 g of Na<sub>2</sub>WO<sub>4</sub>·2H<sub>2</sub>O was used as the tungsten source and dissolved in 30 mL of DI H<sub>2</sub>O under constant stirring at room temperature. Then, 6 mL of 3 M HCl was added drop by drop to form a yellowish precipitate, followed by the addition of 0.20 g of (NH<sub>4</sub>)<sub>2</sub>C<sub>2</sub>O<sub>4</sub> into the above suspension. The cleaned FTO glass substrates were immersed and leaned against the wall of the Teflon-vessel (50 mL volume) with the conducting side facing down. The hydrothermal synthesis was carried out at 120 °C for 12 h. After that, the autoclave was allowed to cool down to room temperature in the oven, then the FTO substrates were taken out and rinsed with DI H<sub>2</sub>O several times and dried at 60 °C in ambient air. The as-prepared yellowish-green thin films were calcined at 500 °C for 1 h in air with a heating rate of 2 °C min<sup>-1</sup>.<sup>[1]</sup>

### 3. Preparation of TiO<sub>2</sub> NRAs substrate

TiO<sub>2</sub> NRAs substrates growing on FTO glass were fabricated by a facile hydrothermal method. The Ti source of titanium butoxide (0.45 mL) was added into a well-mixed solution consisting of HCl (15 mL) and DI H<sub>2</sub>O (15 mL), and then the whole mixture was stirred for another 10 min until the solution became clear. The final formed precursor solution was transferred into a Teflon-lined autoclave (50 mL), meanwhile, the FTO glass was immersed and placed to lean against the wall of autoclave with the conducting side facing

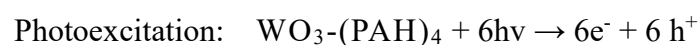
down. The hydrothermal process was carried out at 150 °C for 12 h in an oven. Finally, the FTO substrates with greyish-white thin films were washed with DI H<sub>2</sub>O and dried with a stream of N<sub>2</sub>, and then the films were calcined at 400 °C for 1 h in air with a heating rate of 5 °C min<sup>-1</sup>.<sup>[2]</sup>

#### 4. Preparation of ZnO NRAs substrate

ZnO NRAs substrates growing on FTO glass were prepared via an indirect seed-based hydrothermal growth process. The ZnO seed layers were firstly grown on the FTO glass, wherein Zn(CH<sub>3</sub>COO)<sub>2</sub>·2H<sub>2</sub>O (0.3 M) and ethanolamine (0.3 M) were dissolved into 30 mL of ethanol, and then the FTO glass was immersed into the solution for 5 min and dried at room temperature. The prepared seed layers were calcined at 450 °C for 1 h, leading to form the crystal seeds. The hydrothermal process was taken as the second step, in which the precursor solution was fabricated by adding Zn(NO<sub>3</sub>)<sub>2</sub>·6H<sub>2</sub>O (0.1 M) and methenamine (1 M) into 35 mL of DI H<sub>2</sub>O with a 10 min of stirring. Afterwards, the precursor solution was transferred into a Teflon-lined autoclave (50 mL), and the ZnO seed layer-coated FTO glass was immersed and placed to lean against the wall of autoclave with the conducting side facing down. The hydrothermal process was maintained at 120 °C for 4 h. Finally, the obtained surface-modified FTO substrates were rinsed with DI H<sub>2</sub>O, dried with a stream of N<sub>2</sub>, and calcined at 450 °C for 1 h in air with a heating rate of 5 °C min<sup>-1</sup>.<sup>[3]</sup>

#### 5. Photo-deposition of PbO<sub>2</sub> and Cr<sub>2</sub>O<sub>3</sub> on WO<sub>3</sub>-(PAH)<sub>4</sub>

In the photodeposition experiments, a 300 W Xe lamp (FX300, Beijing Perfect Light Co. Ltd., China) equipped with an AM 1.5 G filter was applied as the light source for simulated sunlight irradiation. The reaction equation of photodeposition is shown as follows:



In typical experiments, stoichiometric precursors (K<sub>2</sub>CrO<sub>4</sub> for Cr<sub>2</sub>O<sub>3</sub> deposition, Pb(NO<sub>3</sub>)<sub>2</sub> for PbO<sub>2</sub>

deposition) were separately mixed with electron donors or acceptors (methanol as an electron donor for  $\text{Cr}_2\text{O}_3$  deposition,  $\text{Na}_2\text{S}_2\text{O}_8$  as an electron acceptor for  $\text{PbO}_2$  deposition) in aqueous solutions (50 mL). The  $\text{WO}_3$ - $(\text{PAH})_4$  sample was then placed in separate photoreactors containing the aforementioned solutions. The sample was subjected to photodeposition under simulated sunlight irradiation. After 2 hours of photodeposition, the sample was removed and washed with DI  $\text{H}_2\text{O}$  for at least 3 times, followed by drying at ambient temperature.

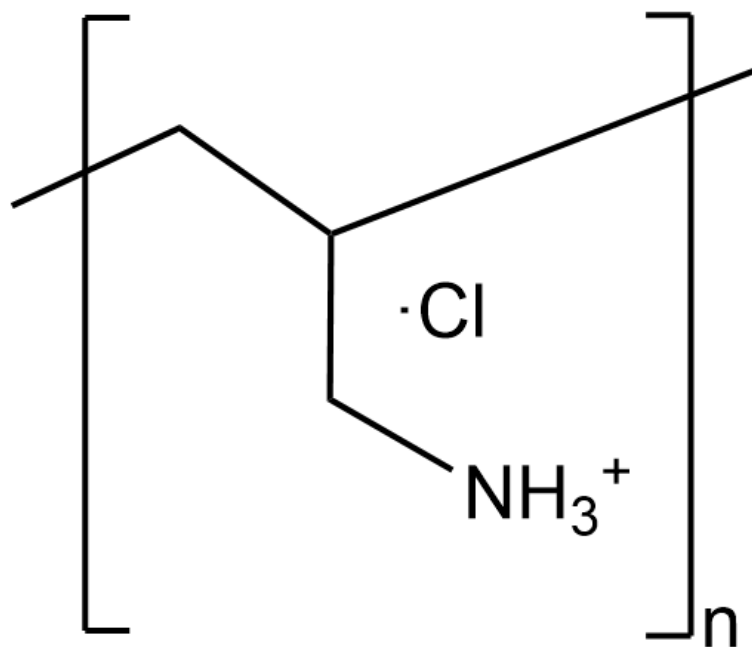


**Figure S1.** Molecular structure of PAH.

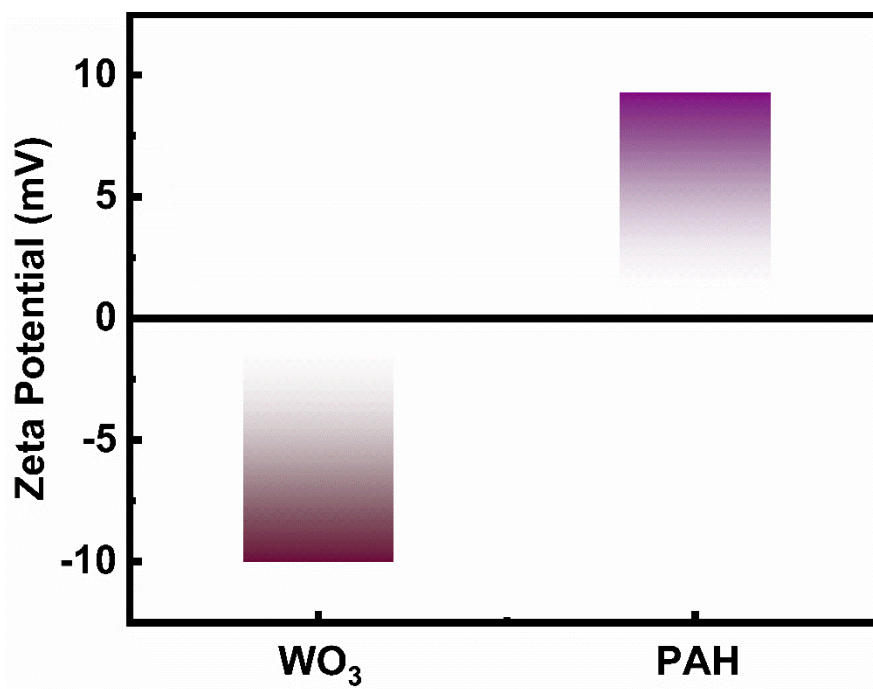
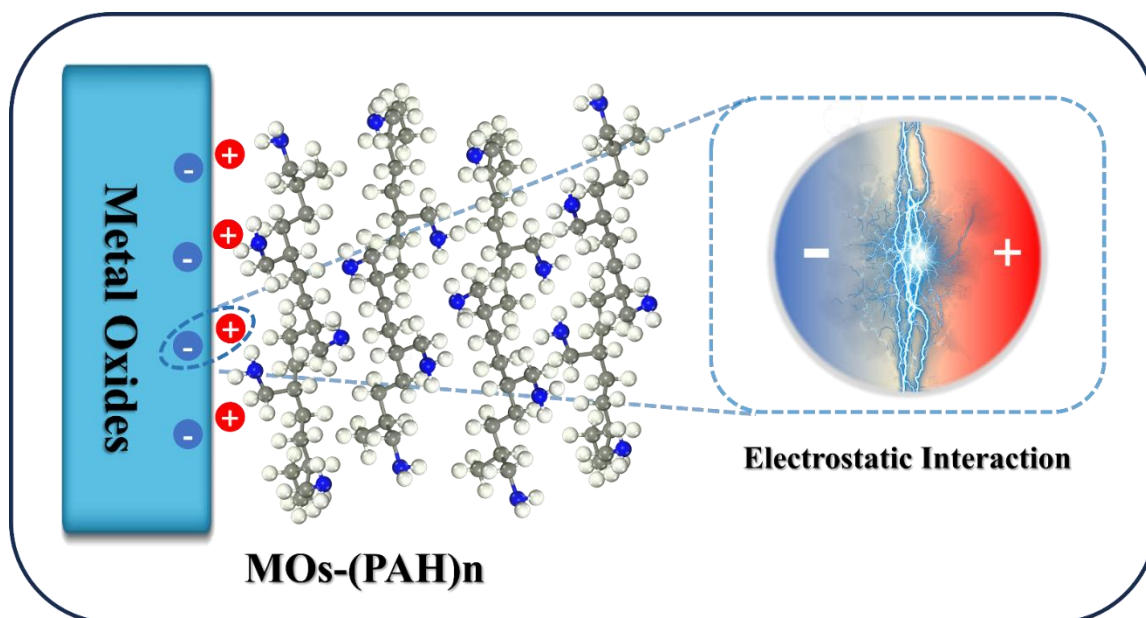
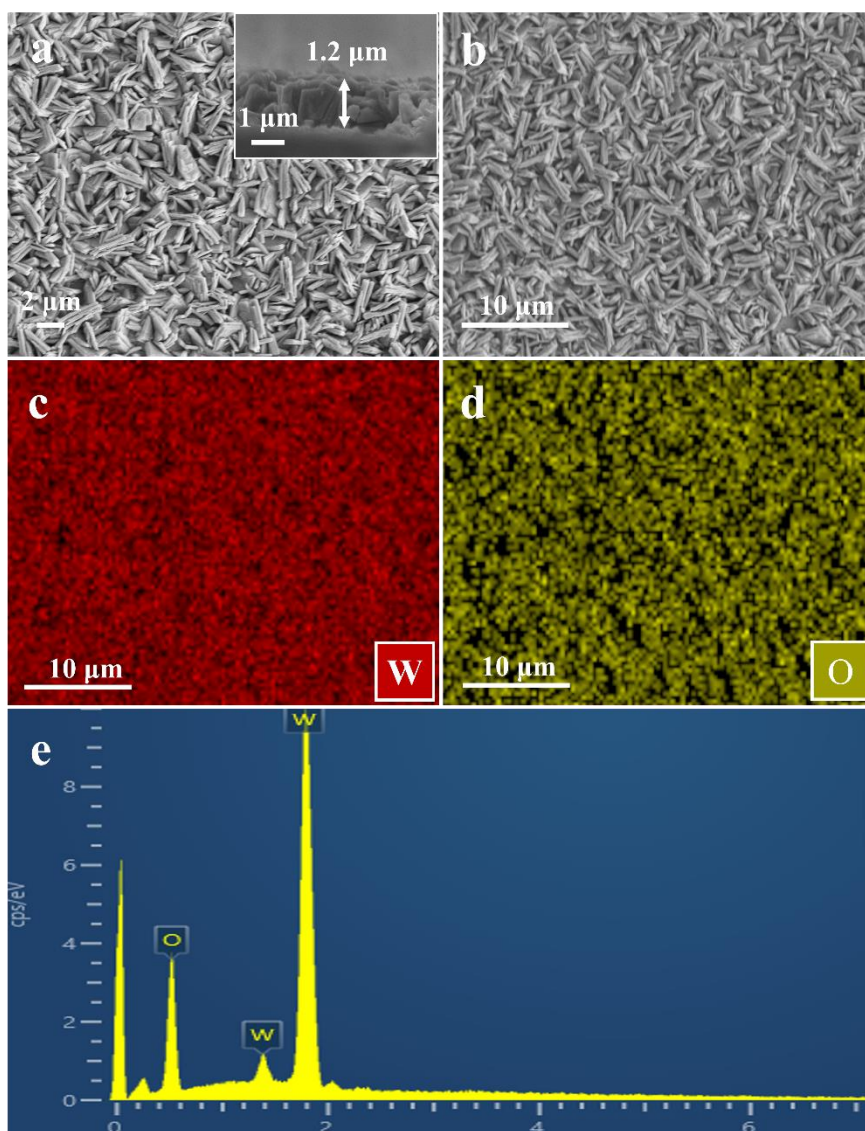


Figure S2. Zeta potentials of WO<sub>3</sub> NRAs and PAH aqueous solution.



**Figure S3.** Schematic illustration of interface configuration between MOs and PAH.



**Figure S4.** (a & b) Top-view and cross-section (inset) SEM images of WO<sub>3</sub> NPAs with (c & d) elemental mapping and (e) EDS results.

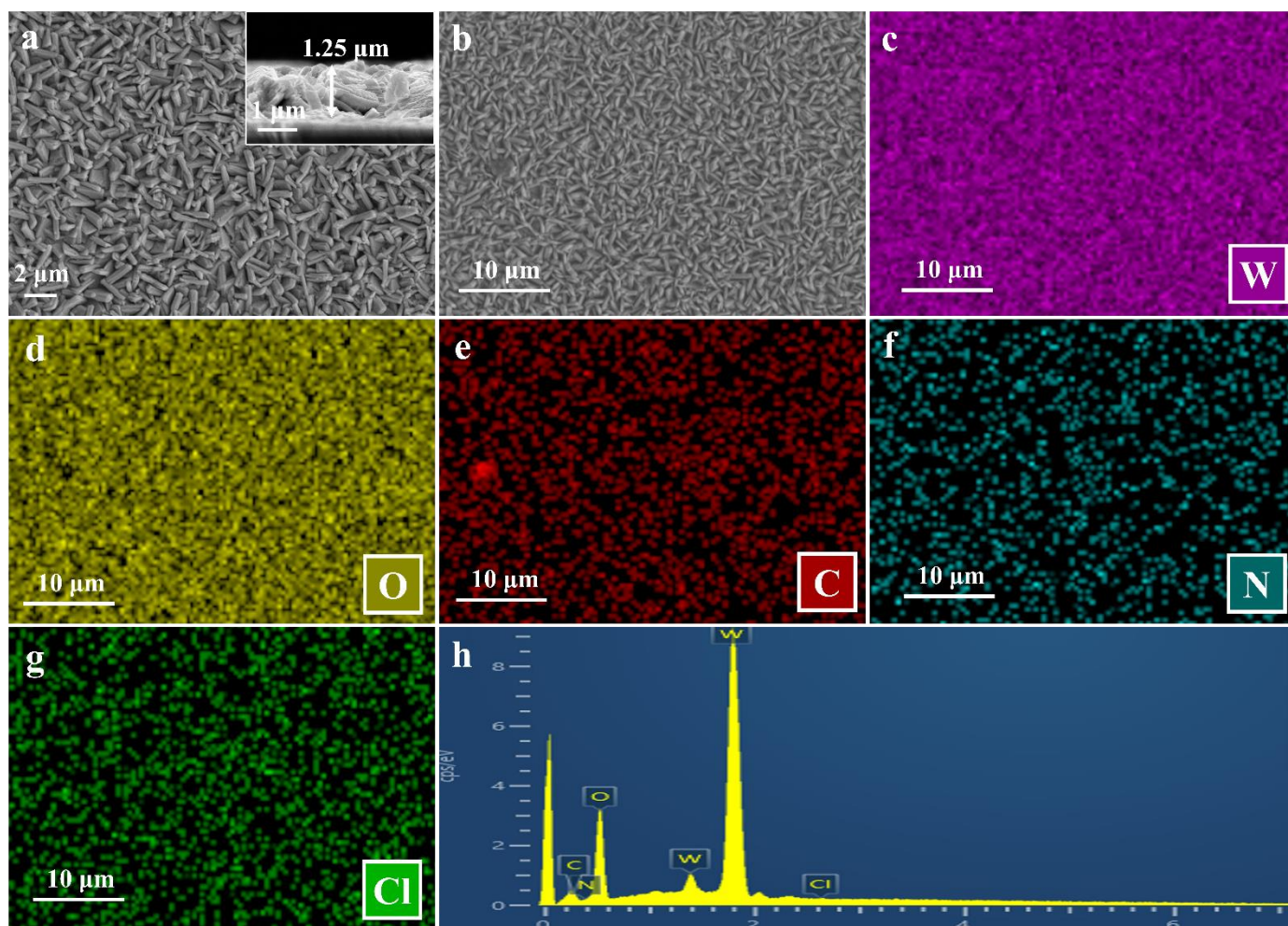


**Figure S5.** (a & b) Top-view and cross-section (inset) SEM images of  $\text{WO}_3\text{-(PAH)}_4$  with (c-g) elemental mapping and (h) EDS results.

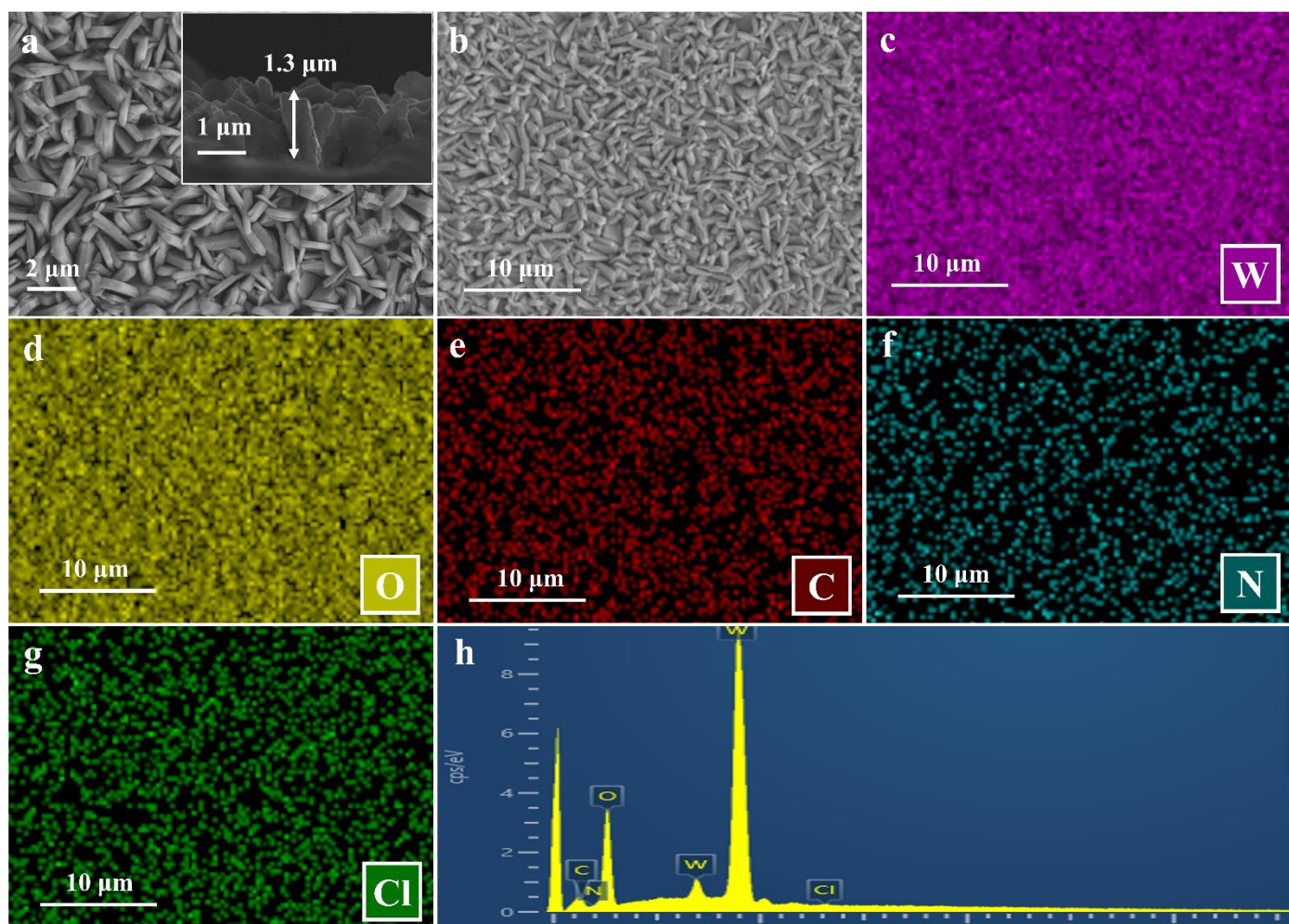


**Figure S6.** (a & b) Top-view and cross-sectional (inset) SEM images of  $\text{WO}_3\text{-(PAH)}_4$ -calcined with (c-g) elemental mapping and (h) EDS results.

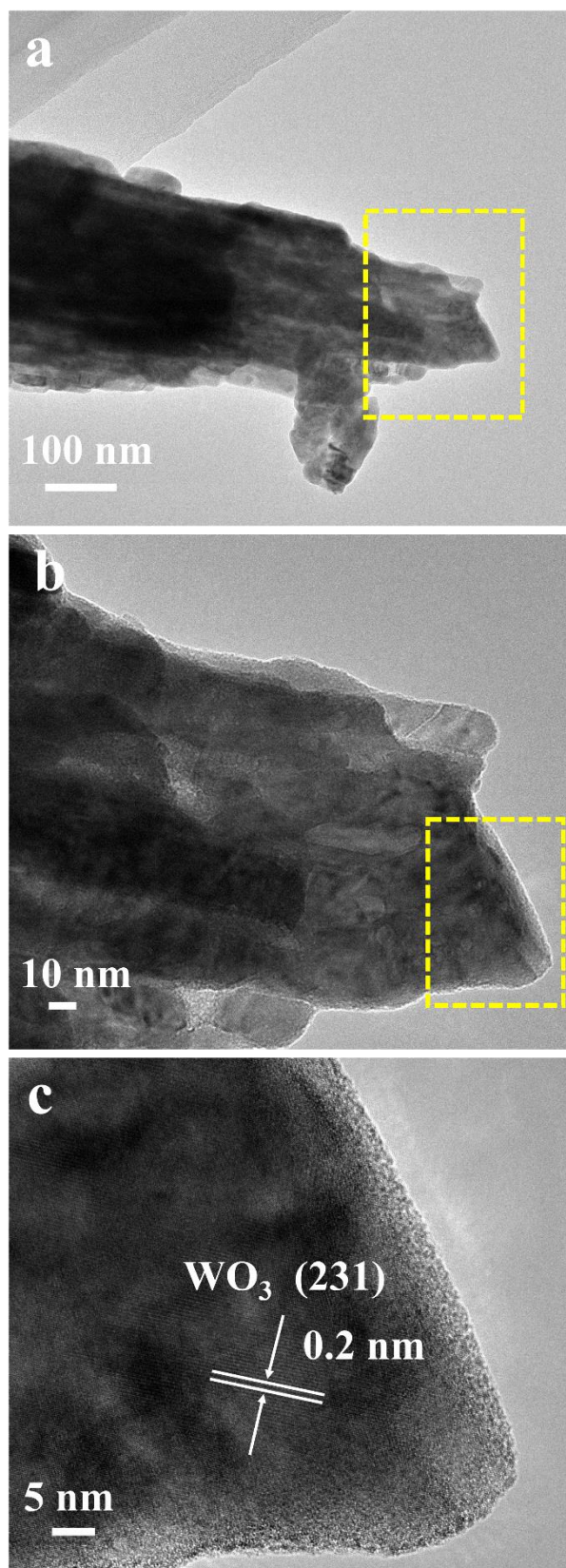


**Figure S7.** TEM and HRTEM images of  $\text{WO}_3$  NPAs.

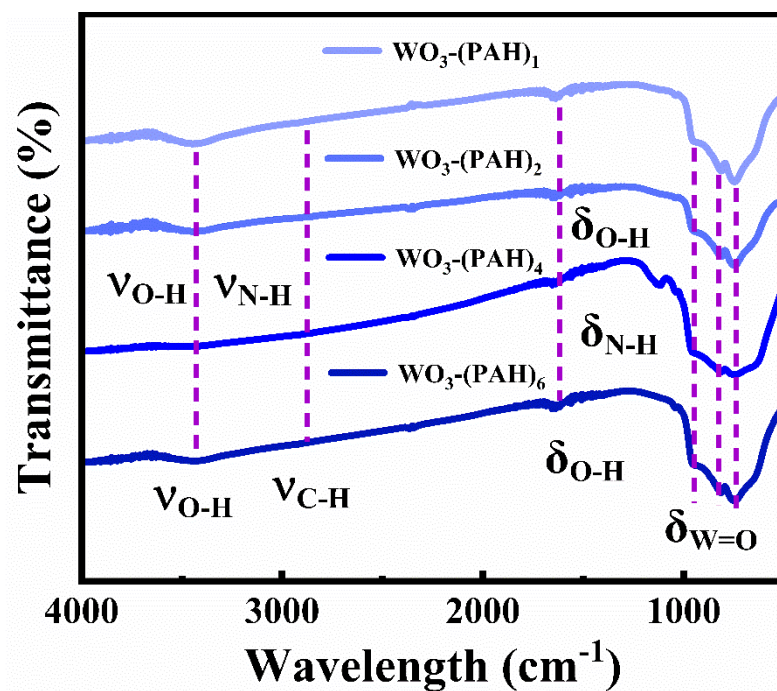


**Figure S8.** FTIR spectra of WO<sub>3</sub>-(PAH)<sub>n</sub> (n = 1, 2, 4, 6) heterostructures with varying assembly number.

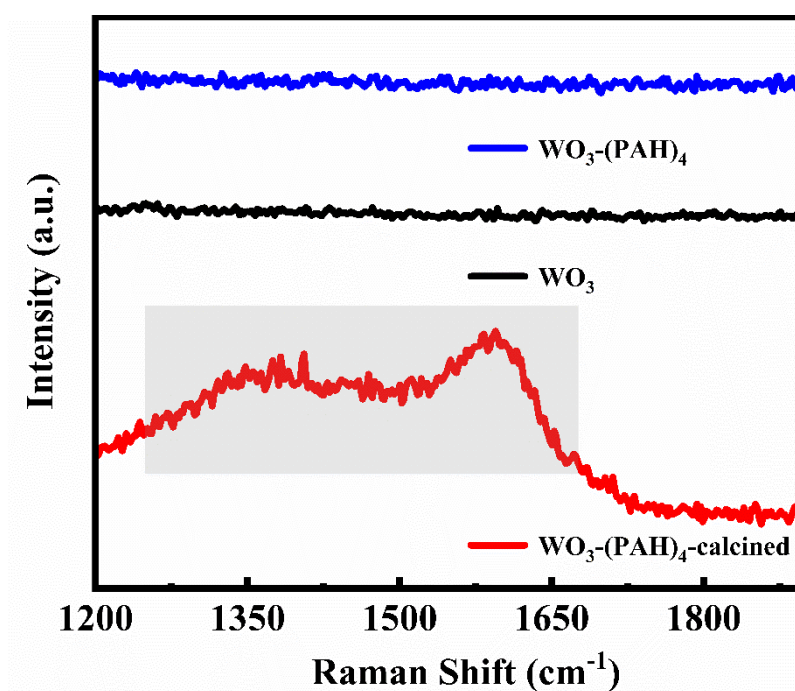


**Figure S9.** Locally magnified Raman spectra of  $\text{WO}_3$ ,  $\text{WO}_3\text{-(PAH)}_4$  and  $\text{WO}_3\text{-(PAH)}_4\text{-calcined}$ .

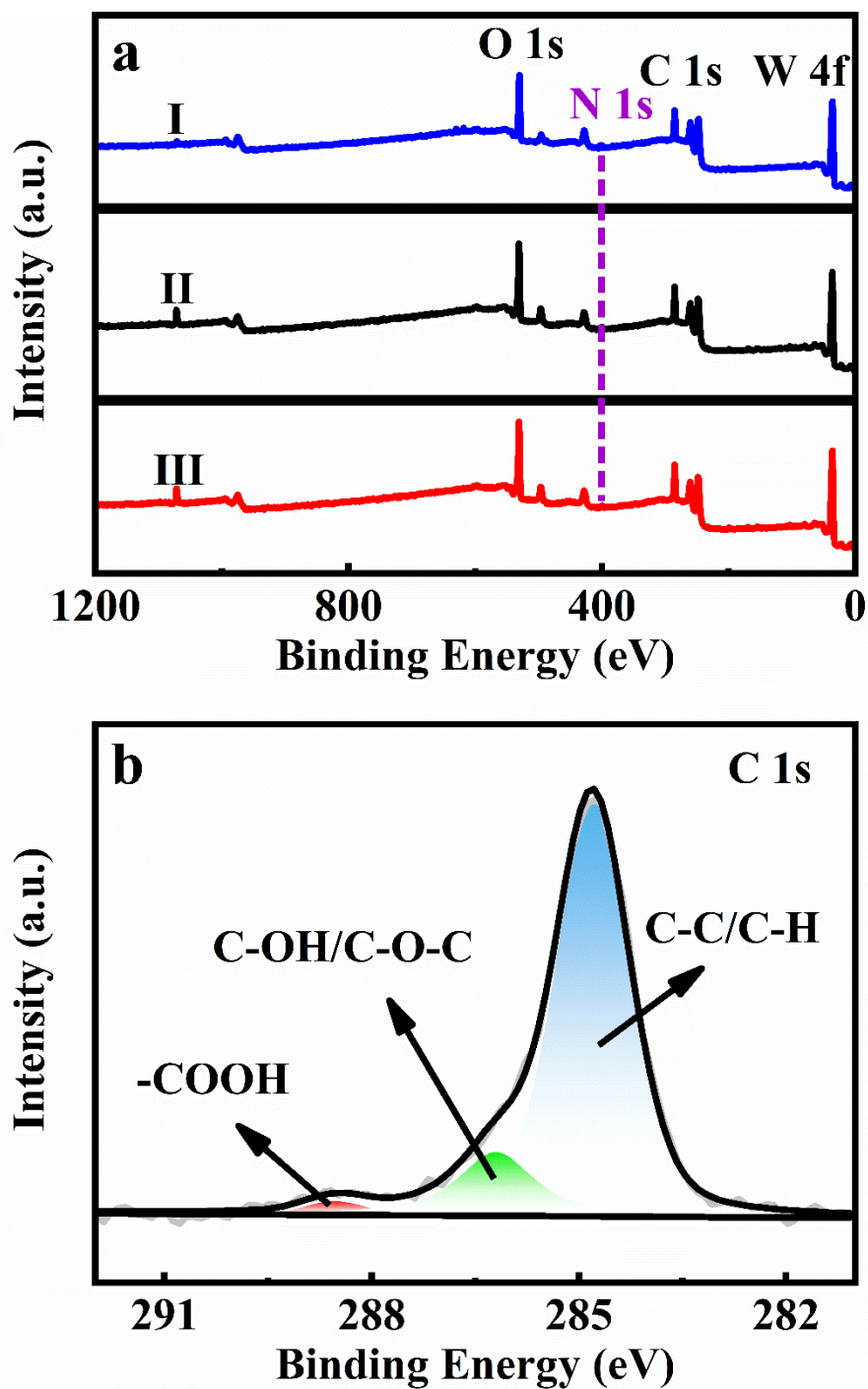


**Figure S10.** (a) Survey spectra of (I)  $\text{WO}_3\text{-(PAH)}_4$ , (II)  $\text{WO}_3$  NPAs & (III)  $\text{WO}_3\text{-(PAH)}_4\text{-calcined}$ , and (b) high-resolution C 1s spectrum of  $\text{WO}_3\text{-(PAH)}_4$ .

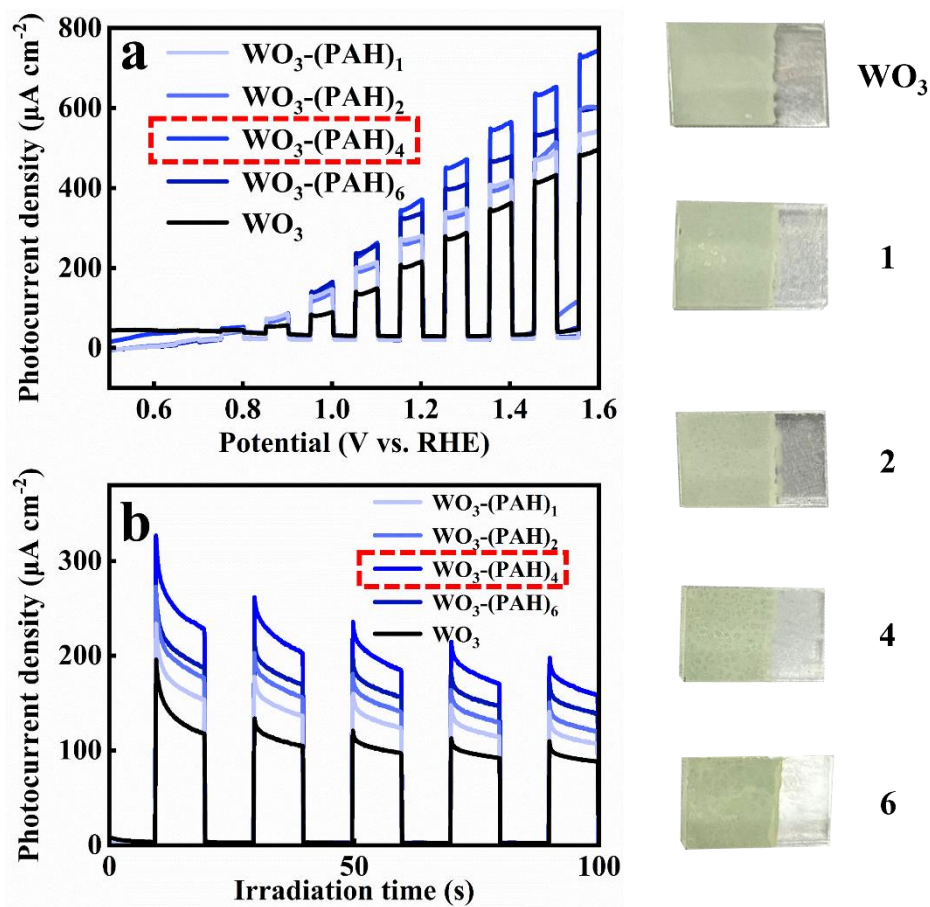


**Figure S11.** (a) LSV results and (b) transient photocurrent responses of  $\text{WO}_3$  and  $\text{WO}_3$ -(PAH)<sub>n</sub> ( $n = 1, 2, 4, 6$ ) multilayered heterostructures under simulated solar light irradiation (AM 1.5G) with photographs on the right side.

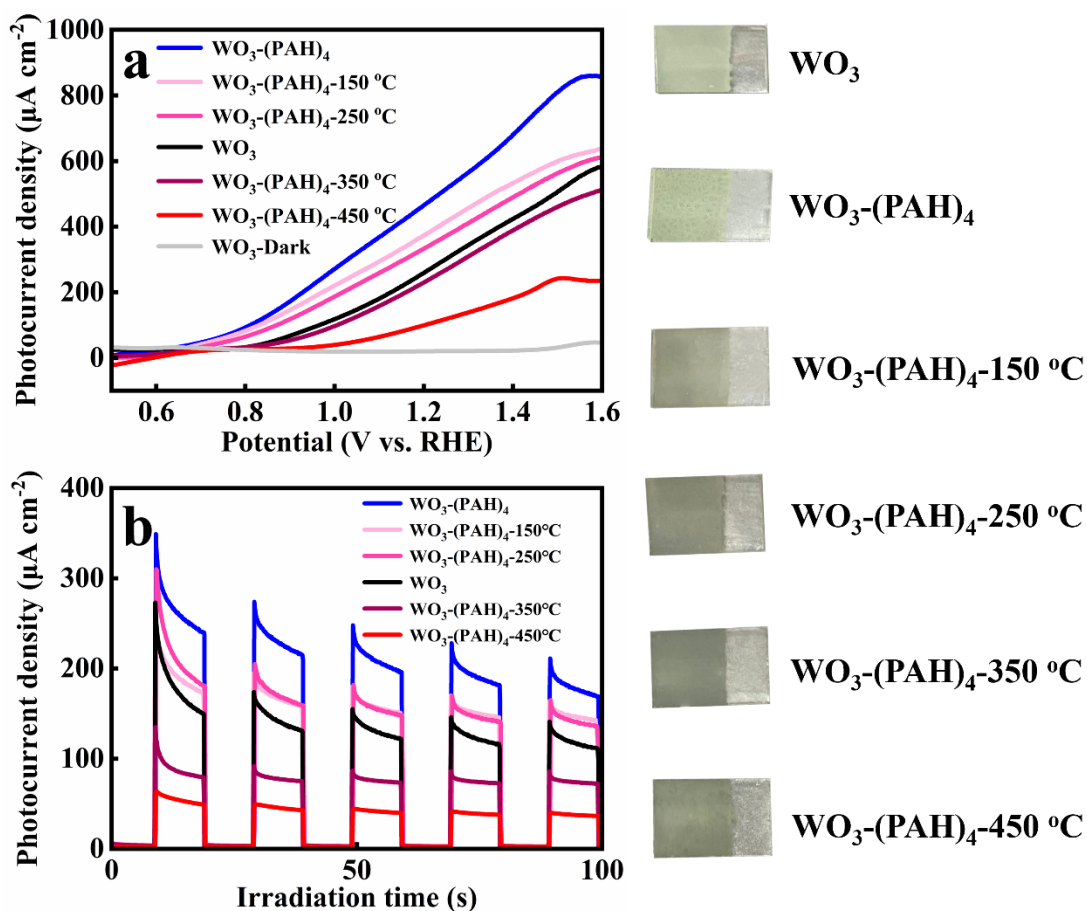


**Figure S12.** (a) LSV results and (b) transient photocurrent responses of  $\text{WO}_3$  and  $\text{WO}_3\text{-(PAH)}_4\text{-X}$  ( $X=150, 250, 350, 450$  °C) heterostructures under simulated solar light irradiation (AM 1.5G) with photographs on the right side.

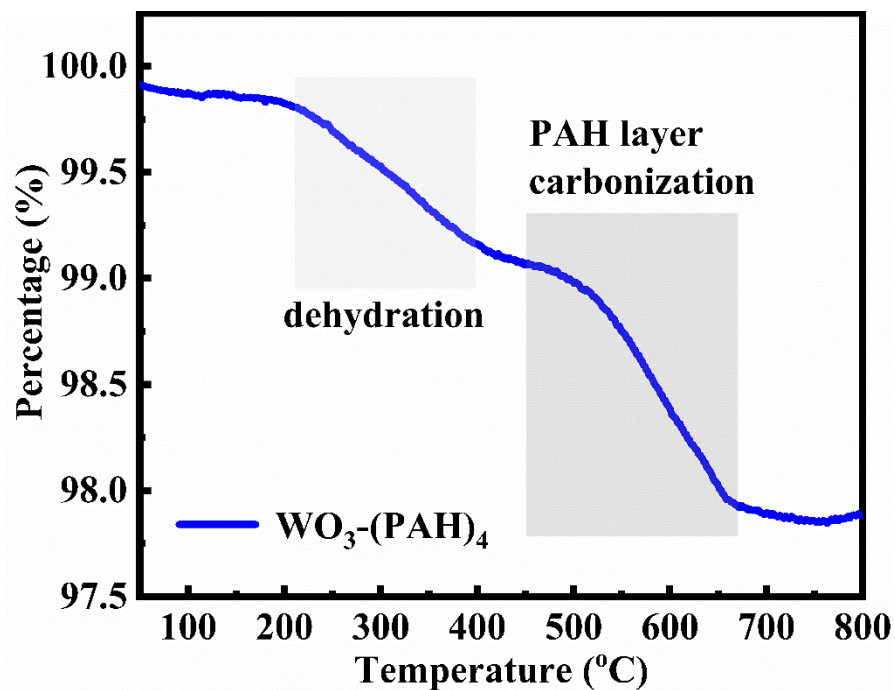


**Figure S13.** TGA curve of  $\text{WO}_3\text{-(PAH)}_4$  heterostructure.

**Note:** Thermogravimetric analyses for  $\text{WO}_3\text{-(PAH)}_4$  were conducted under nitrogen, and the results are summarized in **Figure S13**. The mass loss below 100 °C could be attributed to the removal of adsorbed water. It is noted that  $\text{WO}_3\text{-(PAH)}_4$  shows a two-step thermal degradation process. Starting from around 450 °C, the PAH chain is carbonized and decomposed, with a total loss of 1.2 wt.%.

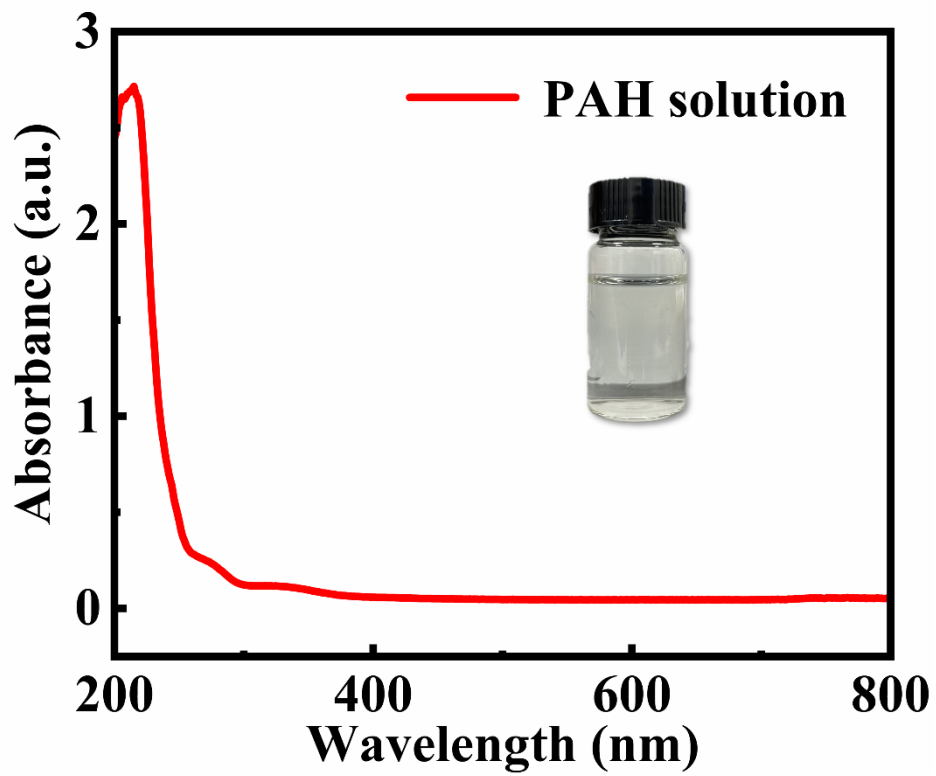
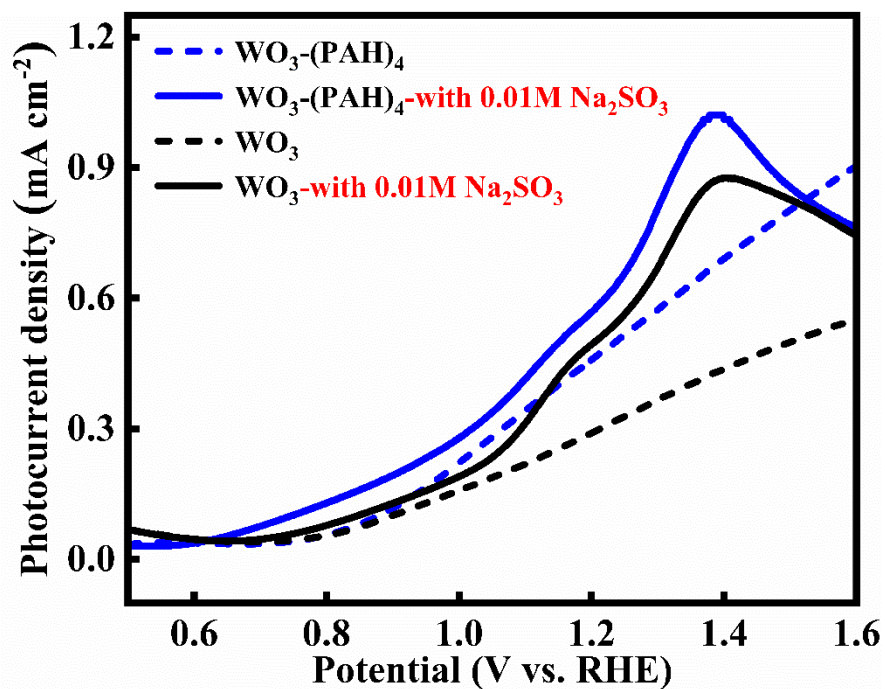
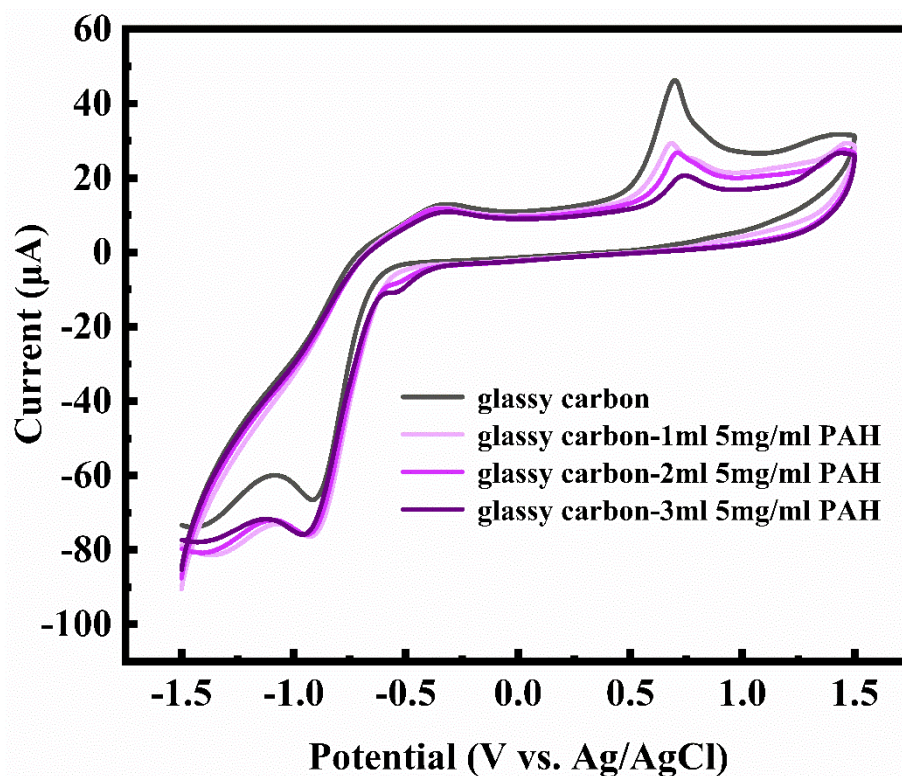


Figure S14. UV-vis absorption spectrum of PAH aqueous solution with photograph in the inset.



**Figure S15.** LSV results of WO<sub>3</sub>-(PAH)<sub>4</sub> and WO<sub>3</sub> NPs in Na<sub>2</sub>SO<sub>4</sub> aqueous solution (0.5 M) with (solid line) and without (dash line) adding Na<sub>2</sub>SO<sub>3</sub> (0.01 M) under simulated solar light irradiation (AM 1.5G).



**Figure S16.** CV curves of PAH with different addition amount (1, 2, 3ml 5mg/mL) for scanning range of -1.5~1.5V vs. Ag/AgCl. (electrolyte: degassed acetonitrile containing 0.1 M tetrabutylammonium perchlorate)

**Note:** As shown in **Figure S15**, CV curves of PAH do not show the oxidation and reduction peaks, confirming that the molecular structure of PAH does not possess the  $\pi$ -conjugated structure, and thus suggests that it is indeed an insulating polymer in a solid state.

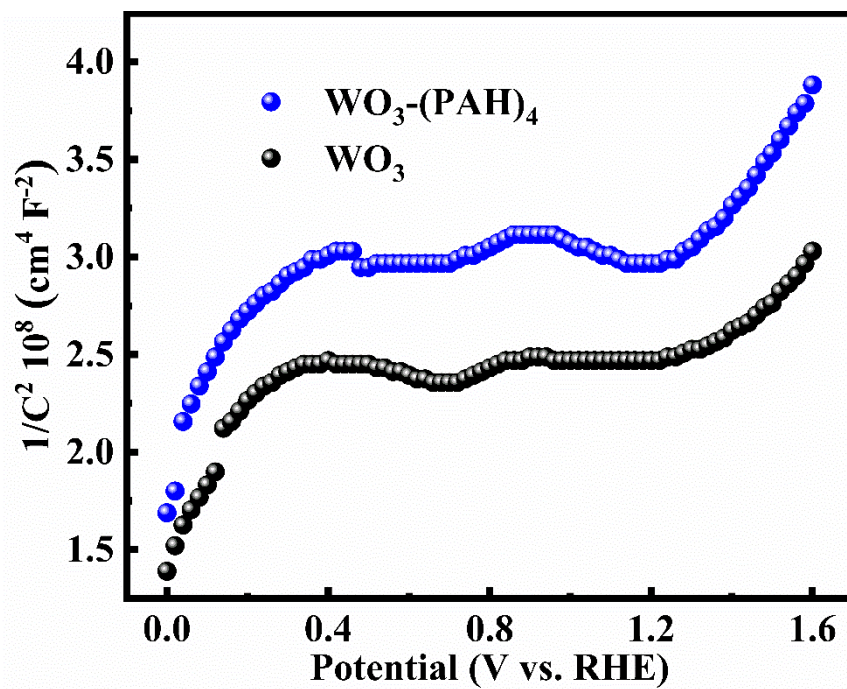
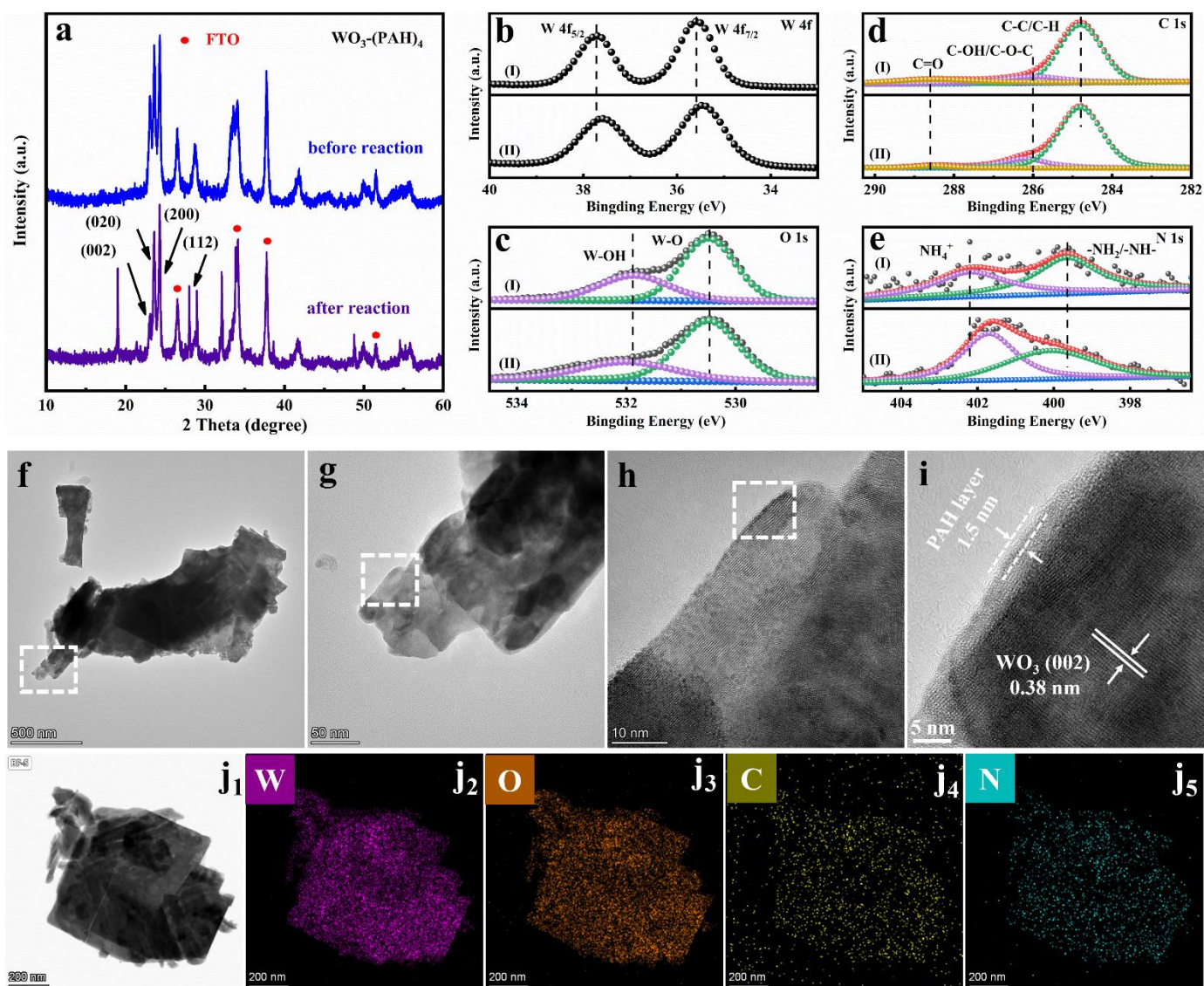


Figure S17. Mott-Schottky plots of  $\text{WO}_3\text{-(PAH)}_4$  and  $\text{WO}_3$ .



**Figure S18.** (a) After reaction and before reaction XRD results of  $\text{WO}_3\text{-(PAH)}_4$ . (I) After reaction and (II) before reaction high-resolution (b) W 4f, (c) O 1s, (d) C 1s and (e) N 1s spectra of  $\text{WO}_3\text{-(PAH)}_4$ . After reaction TEM and HRTEM images of (f-i)  $\text{WO}_3\text{-(PAH)}_4$  with (j1 - j5) elemental mapping results of  $\text{WO}_3\text{-(PAH)}_4$ .

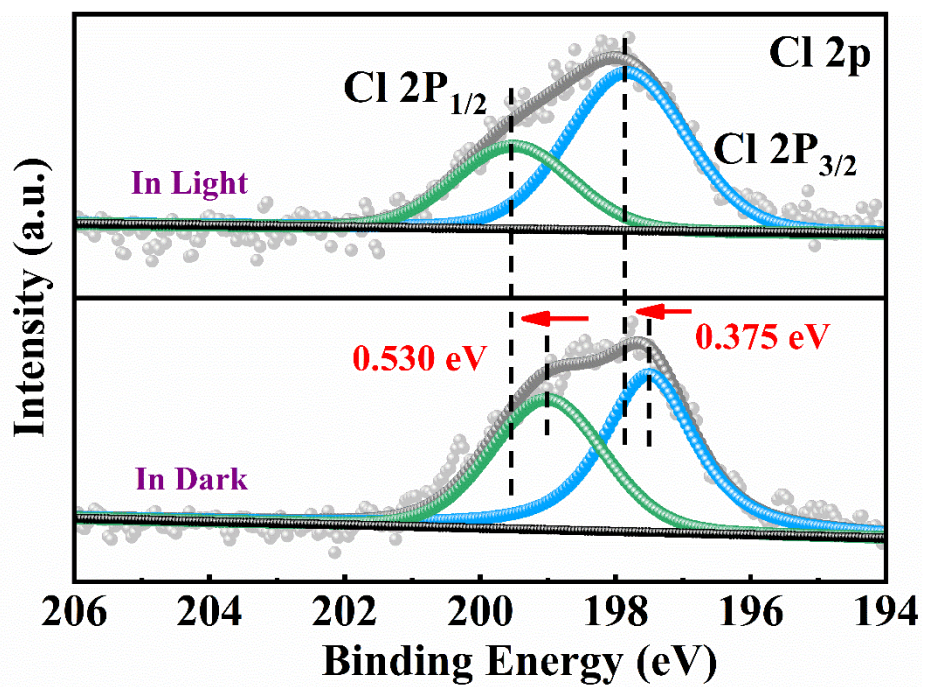
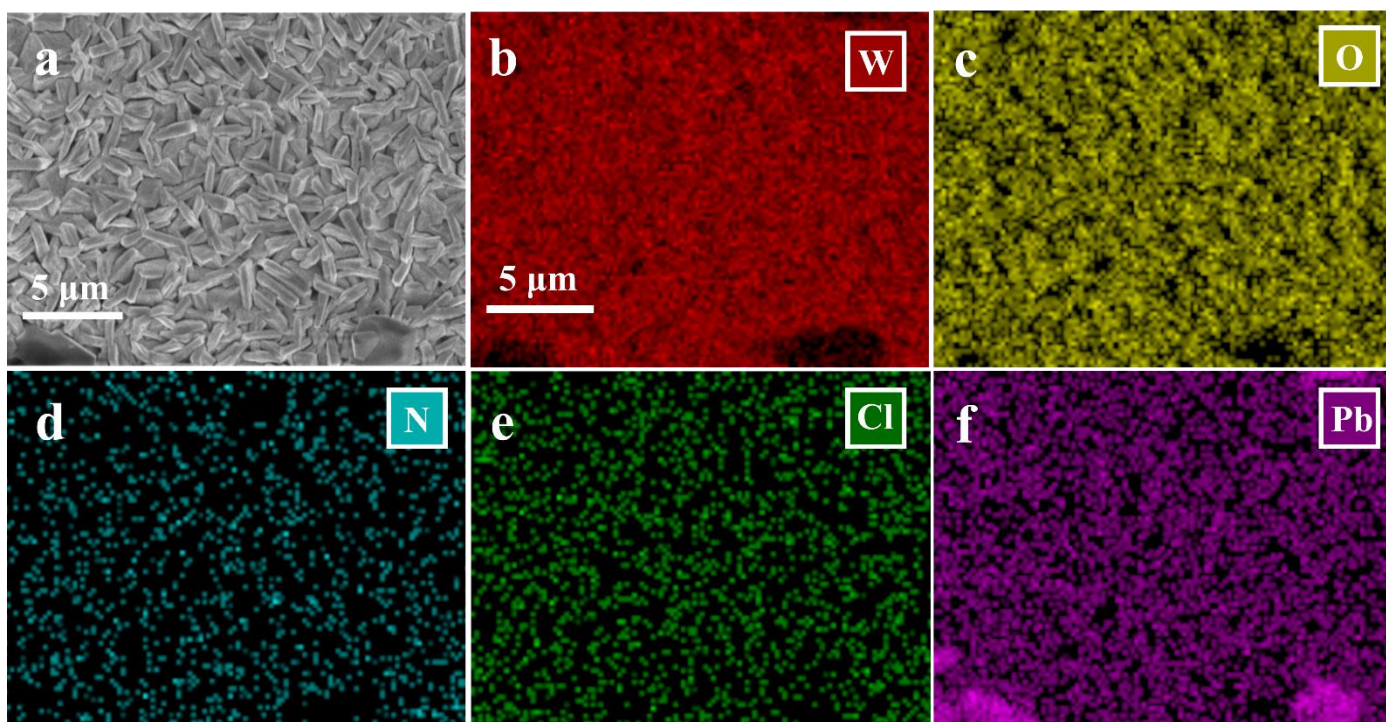
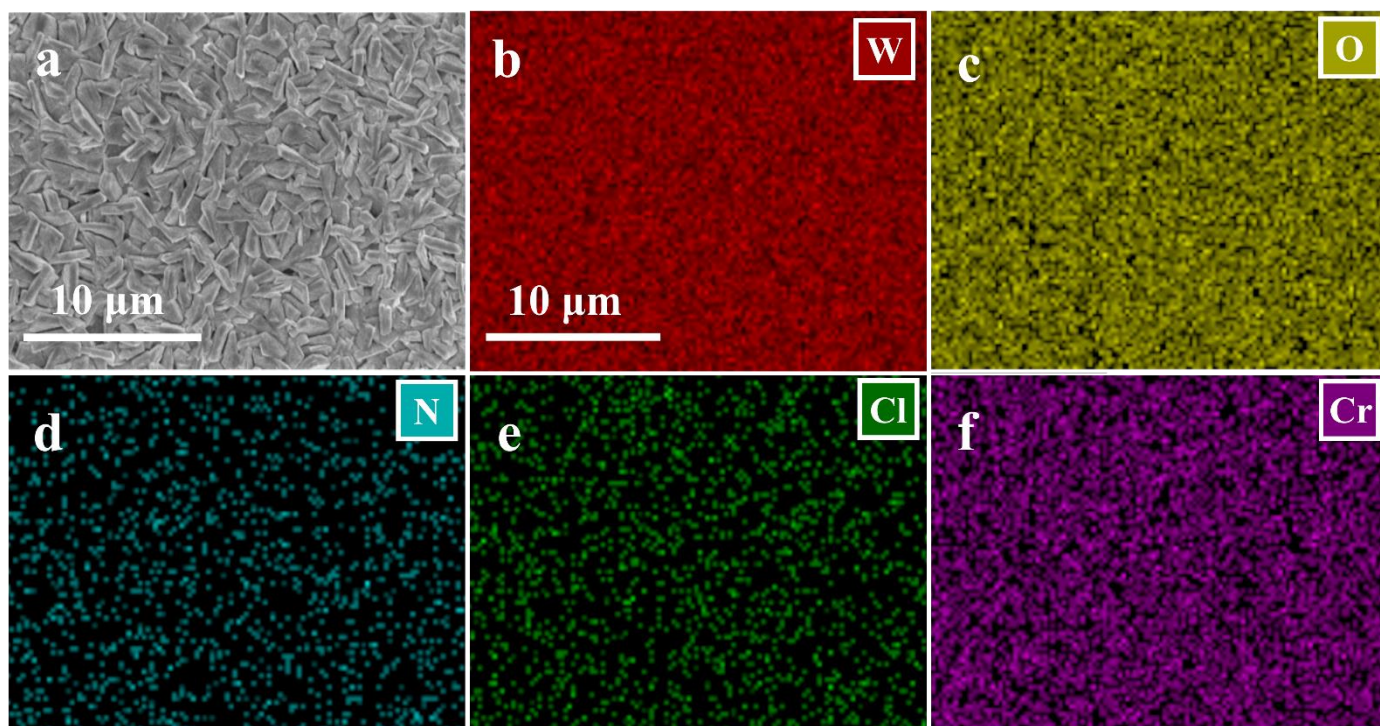


Figure S19. In-situ irradiated high-resolution XPS spectra of Cl 2p for WO<sub>3</sub>-(PAH)<sub>4</sub>.



**Figure S20.** (a) Top-view SEM images of photodeposited  $\text{PbO}_2$  on the  $\text{WO}_3$ - $(\text{PAH})_4$  with (b-f) elemental mapping result.



**Figure S21.** (a) Top-view SEM images of  $\text{Cr}_2\text{O}_3$  photo-deposited on the  $\text{WO}_3\text{-(PAH)}_4$  with (b-f) elemental mapping result.

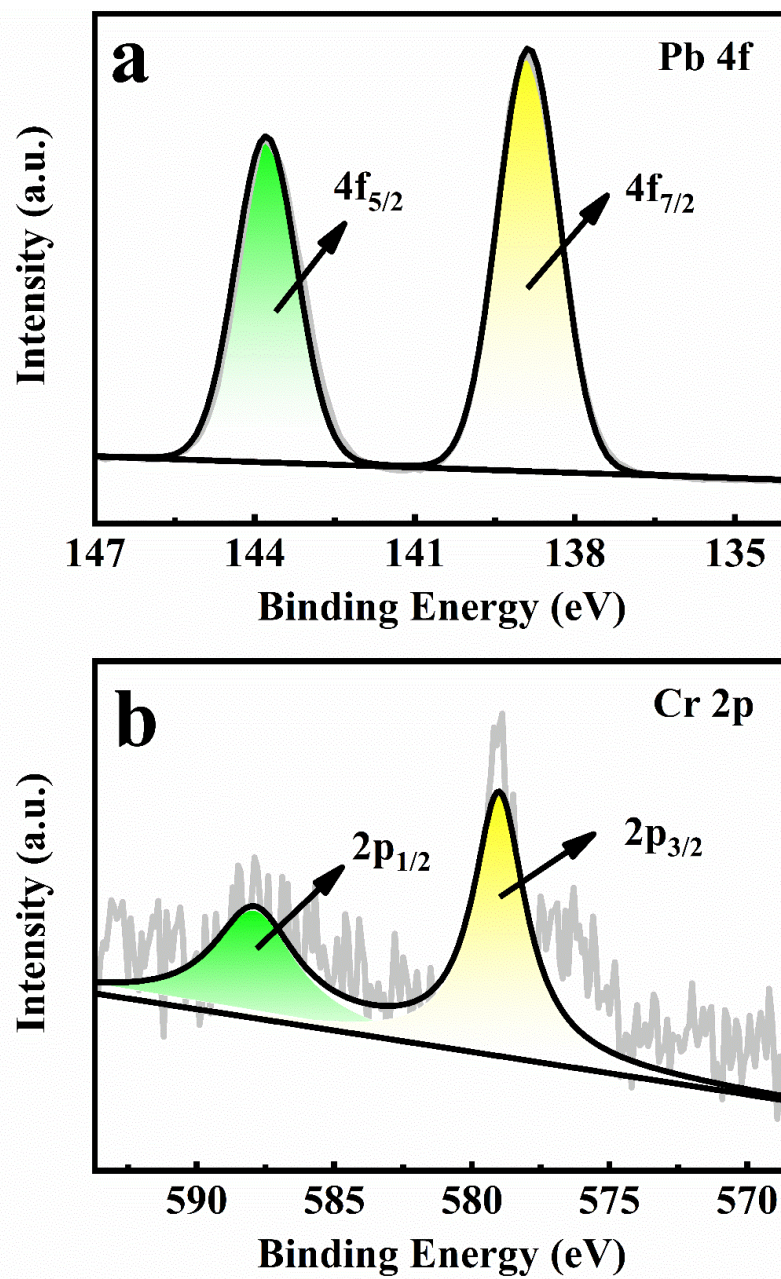


**Figure S22.** High-resolution (a) Pb 4f spectra of  $\text{PbO}_2$  and (b) Cr 2p spectra of  $\text{Cr}_2\text{O}_3$ .

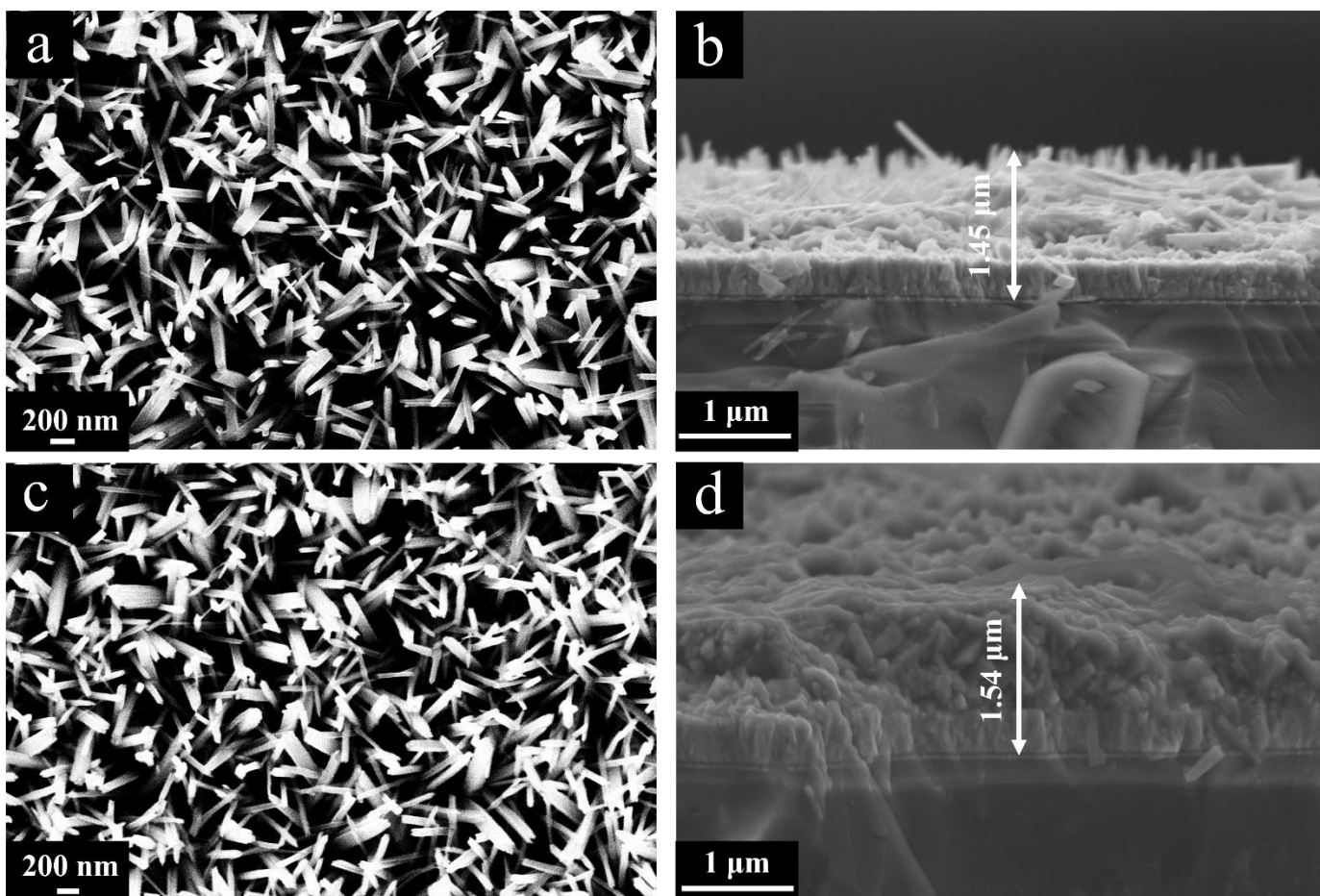


**Figure S23.** Top-view SEM images of (a) TiO<sub>2</sub> NRAs and (c) TiO<sub>2</sub>-(PAH)<sub>4</sub>; Cross-sectional SEM images of (b) ZnO NRAs and (d) ZnO-(PAH)<sub>4</sub>.

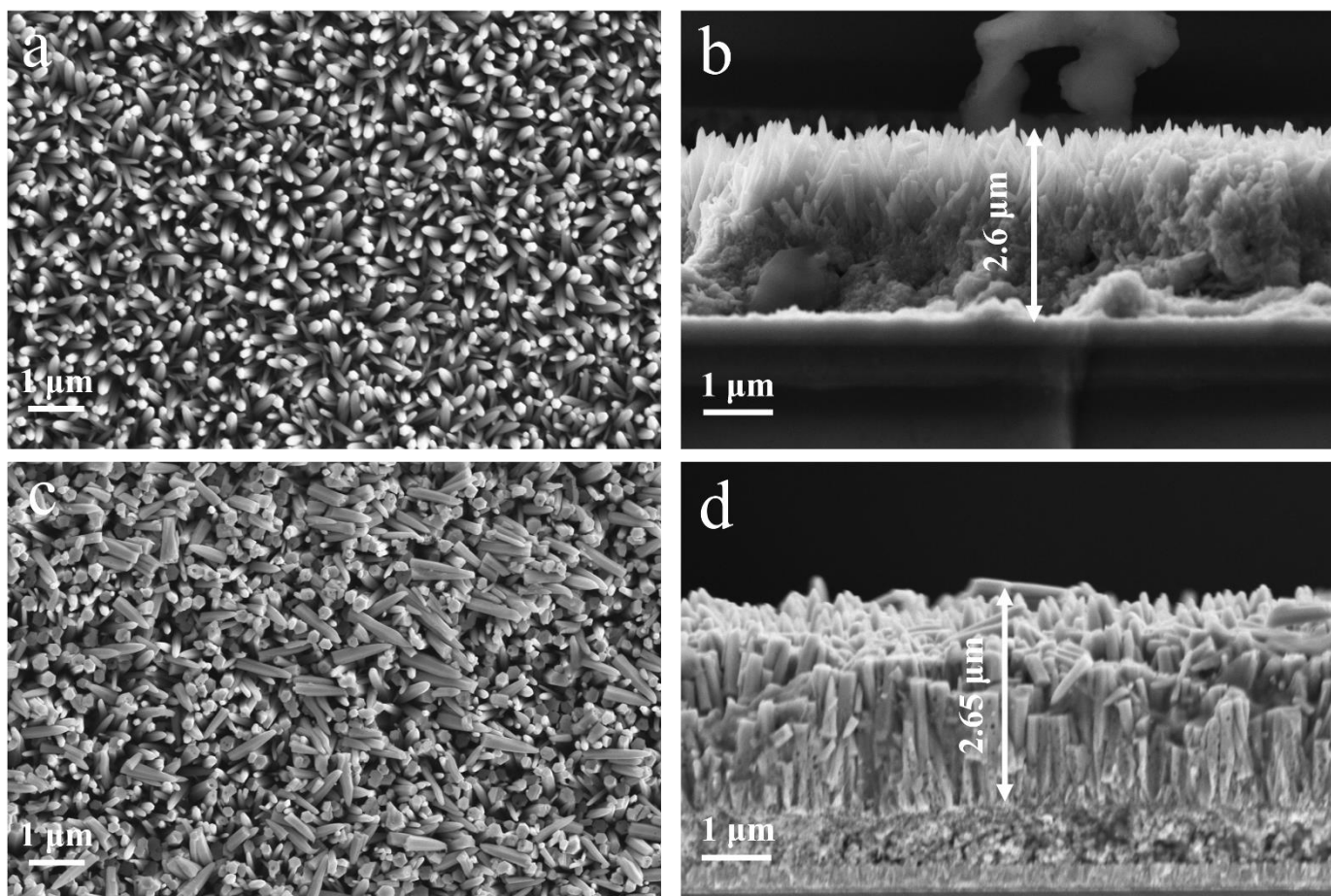


**Figure S24.** Top-view SEM images of (a) ZnO NRAs and (c) ZnO-(PAH)<sub>4</sub>; Cross-sectional SEM images of (b) ZnO NRAs and (d) ZnO-(PAH)<sub>4</sub>.

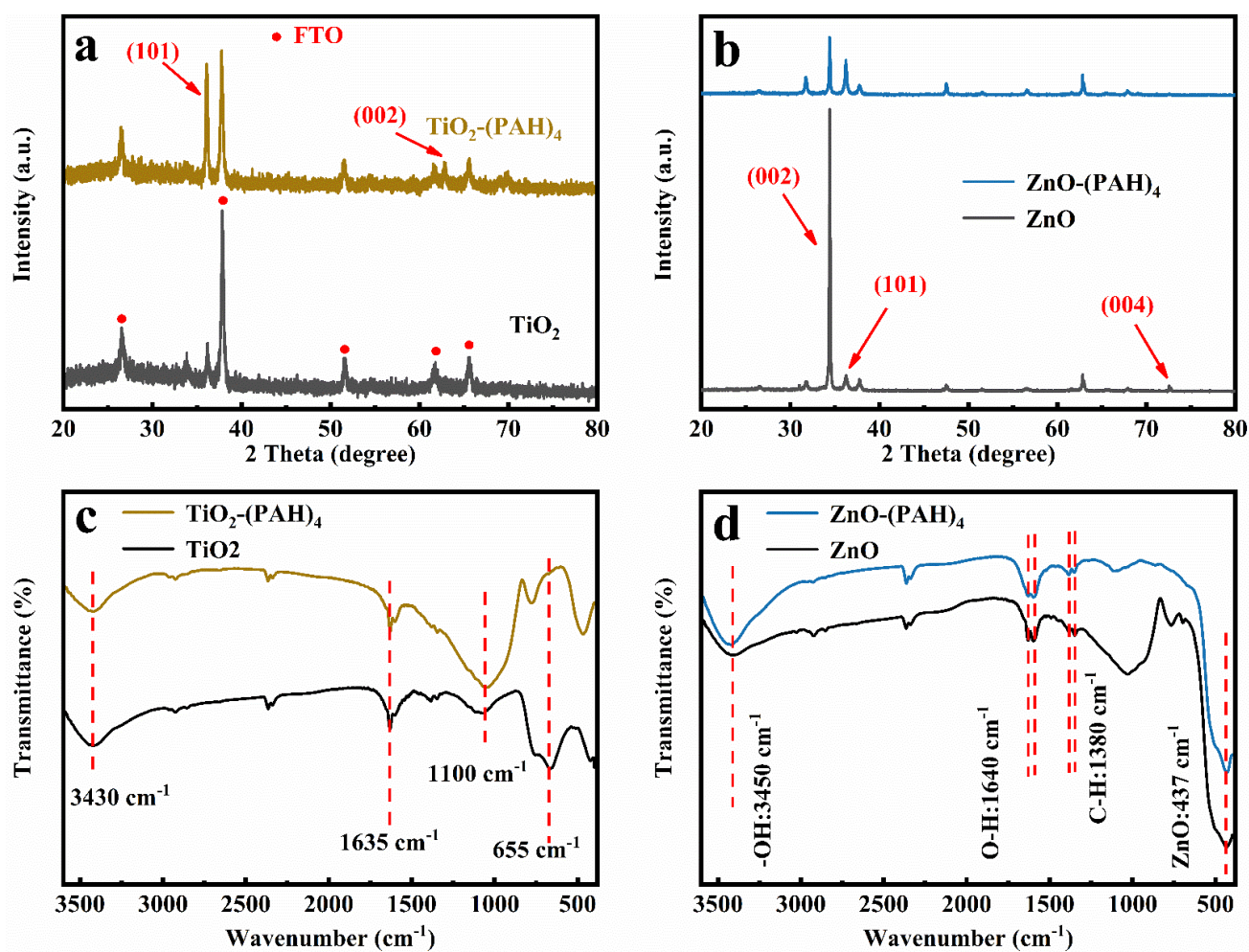


**Figure S25.** XRD patterns of (a) TiO<sub>2</sub> NRAs & TiO<sub>2</sub>-(PAH)<sub>4</sub> and (b) ZnO NRAs & ZnO-(PAH)<sub>4</sub>; FTIR spectra of (c) TiO<sub>2</sub> NRAs, TiO<sub>2</sub>-(PAH)<sub>4</sub> and (d) ZnO NRAs, ZnO-(PAH)<sub>4</sub>.

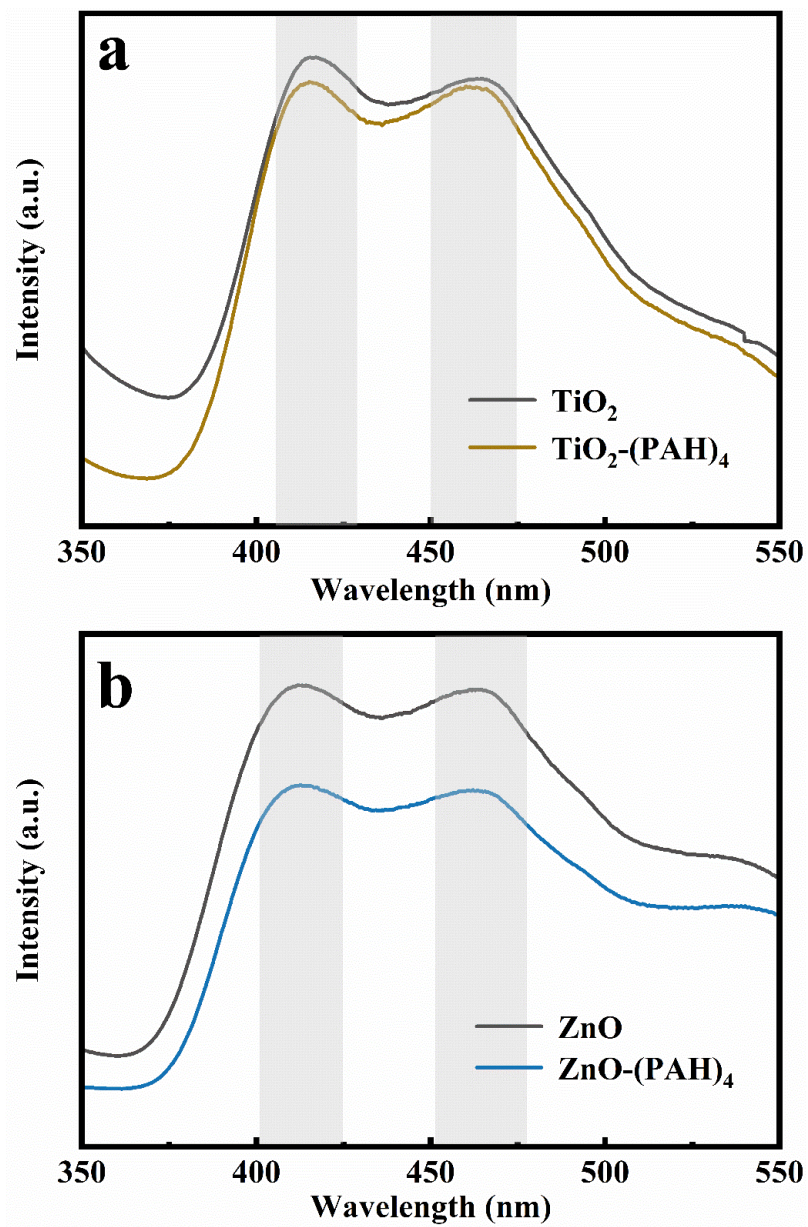
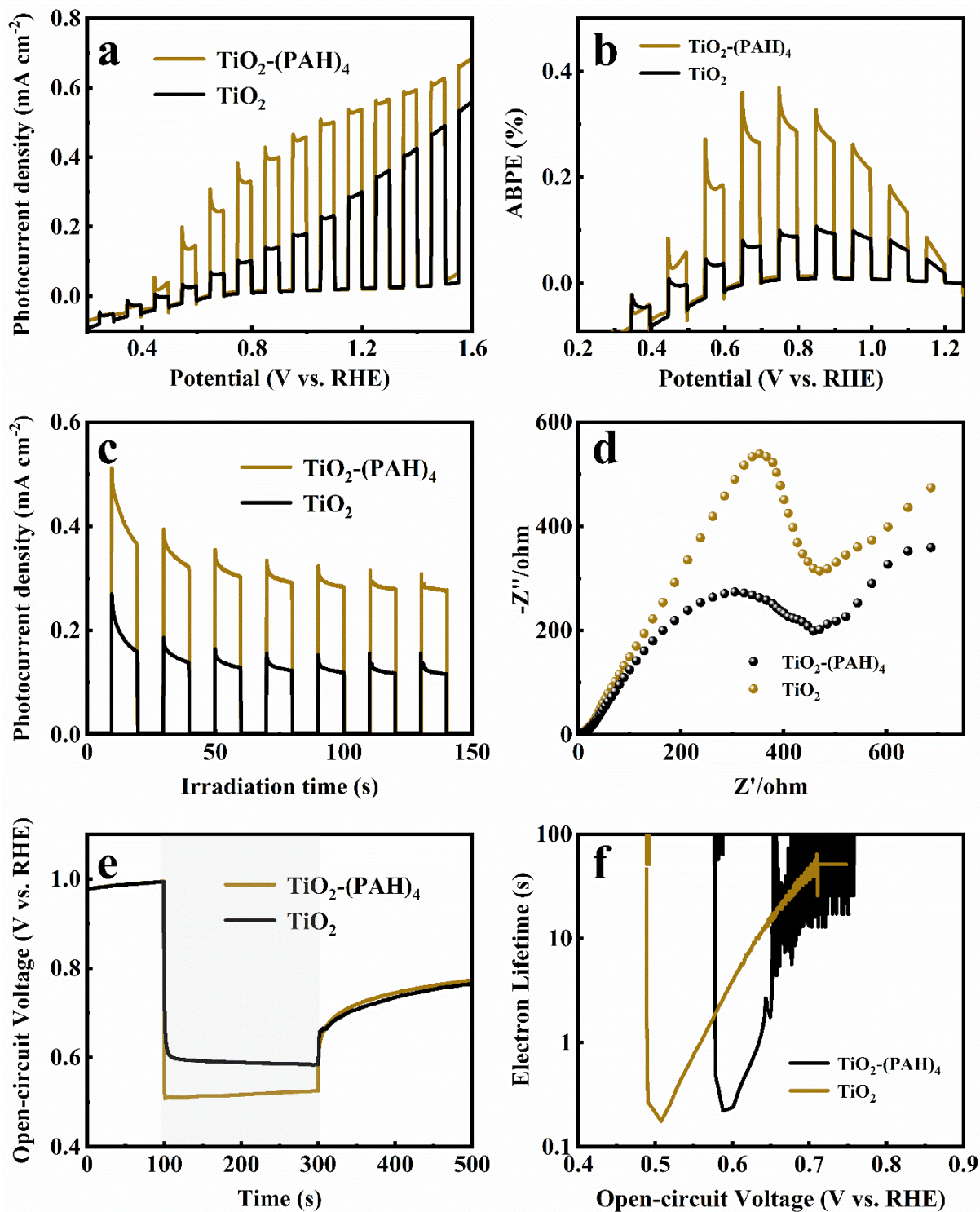
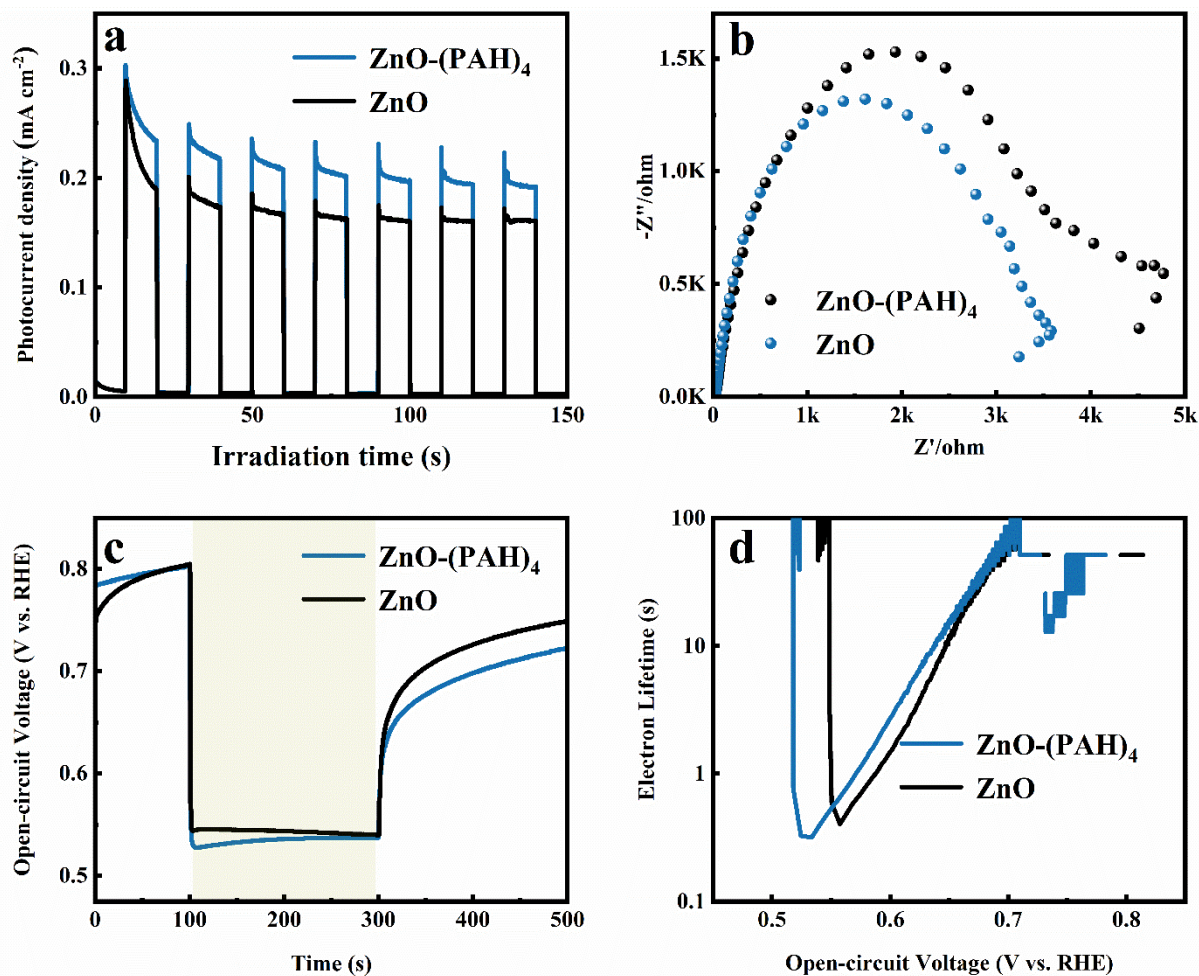


Figure S26. PL spectra of (a)  $\text{TiO}_2$  NRAs &  $\text{TiO}_2\text{-(PAH)}_4$  and (b)  $\text{TiO}_2$  NRAs &  $\text{TiO}_2\text{-(PAH)}_4$ .



**Figure S27.** (a) LSV (scan rate:  $5 \text{ mV s}^{-1}$ ) & (b) ABPE, (c) I-t (bias: 1.0 V vs. RHE), (d) EIS results (amplitude: 10 mV, frequency:  $10^{-5}$  to 0.01 Hz), (e) OCVD & (f) electron lifetime of  $\text{TiO}_2$  NRAs and  $\text{TiO}_2$ -(PAH)<sub>4</sub>. All the PEC results were measured utilizing  $\text{Na}_2\text{SO}_4$  aqueous solution (0.5 M, pH = 7) as the electrolyte under simulated sunlight irradiation (AM 1.5G).



**Figure S28.** (a) I-t (bias: 1.0 V vs. RHE), (b) EIS results (amplitude: 10 mV, frequency: 10<sup>-5</sup> to 0.01 Hz), (c) OCVD & (d) electron lifetime of ZnO NRAs and ZnO-(PAH)<sub>4</sub>. All the PEC results were measured utilizing Na<sub>2</sub>SO<sub>4</sub> aqueous solution (0.5 M, pH = 7) as the electrolyte under simulated sunlight irradiation (AM 1.5G).

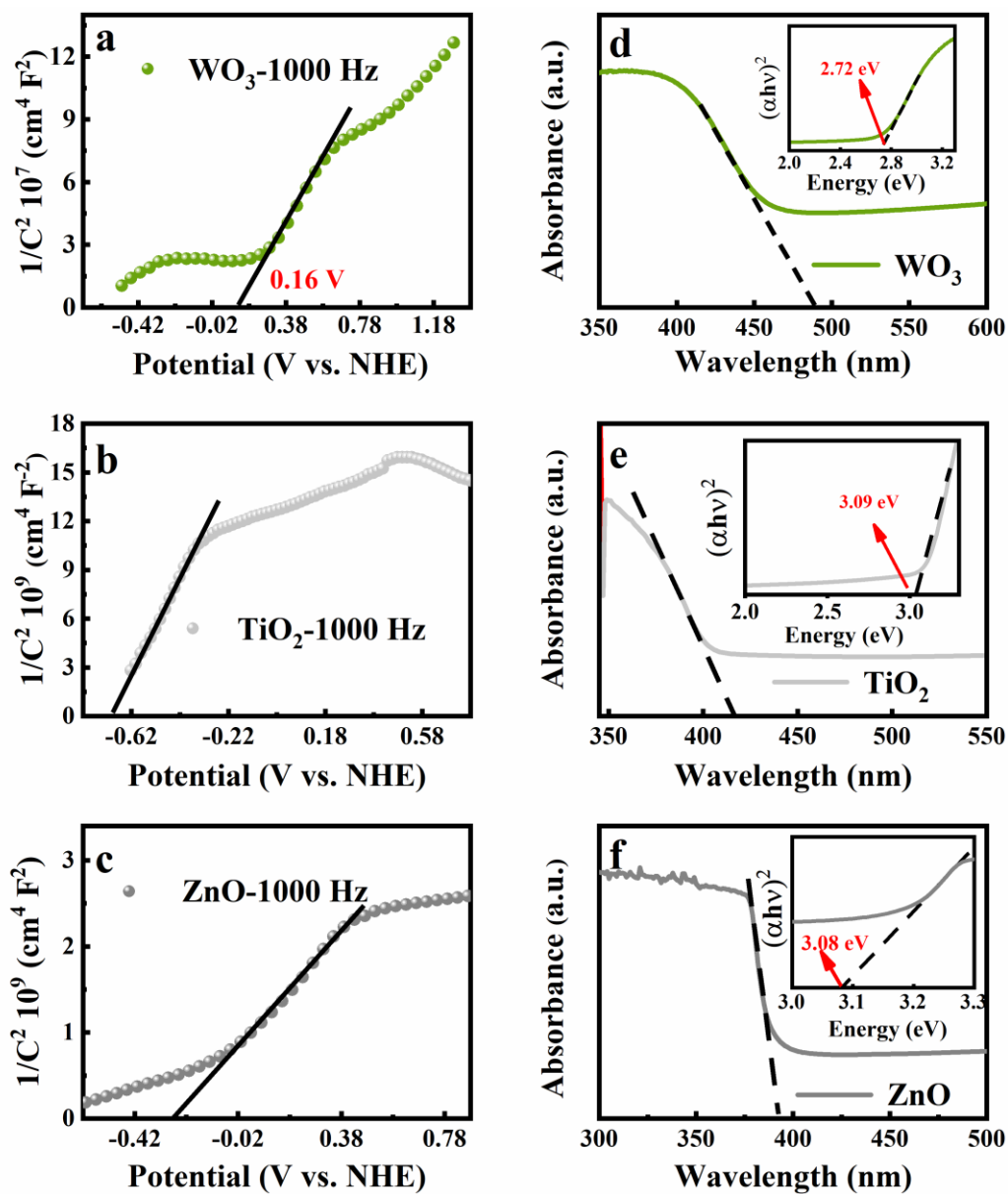


**Figure S29.** M-S results of (a)  $\text{WO}_3$ , (b)  $\text{TiO}_2$  and (c)  $\text{ZnO}$  at 1000 Hz; DRS results of (d)  $\text{WO}_3$ , (e)  $\text{TiO}_2$  and (f)  $\text{ZnO}$  with corresponding plots of transformed Kubelka-Munk function vs. energy of light in the insets.

**Table S1.** Peak position with corresponding functional groups for photoanodes.

<i>Peak position (cm<sup>-1</sup>)</i>	<i>WO<sub>3</sub>-(PAH)<sub>4</sub></i>	<i>WO<sub>3</sub></i>	<i>WO<sub>3</sub>-(PAH)<sub>4</sub>-450 °C</i>
<b>3460<sup>[4]</sup></b>	<b>VO-H</b>	<b>VO-H</b>	<b>VO-H</b>
	<b>VN-H</b>		<b>VN-H</b>
<b>2922<sup>[4b, 5]</sup></b>	<b><i>ν</i><sub>C-H</sub></b>	<b>N.D.</b>	<b><i>ν</i><sub>C-H</sub></b>
<b>1635<sup>[4]</sup></b>	<b>δO-H</b>	<b>δO-H</b>	<b>δO-H</b>
	<b>δN-H</b>		<b>δN-H</b>
	<b>δC=O</b>		<b>δC=O</b>
<b>965, 836 &amp; 766<sup>[6]</sup></b>	<b><i>δ</i><sub>W=O</sub></b>	<b>δ<sub>W=O</sub></b>	<b>δ<sub>W=O</sub></b>

N.D.: Not Detected.

*ν*: Stretching vibration.

δ: Deformation vibration.

**Table S2.** Chemical bond species vs. B.E. for different photoelectrodes.

<i>Element</i>	<i>WO<sub>3</sub></i>	<i>WO<sub>3</sub>-(PAH)<sub>4</sub></i>	<i>WO<sub>3</sub>-(PAH)<sub>4</sub>-450 °C</i>	<i>Chemical Bond Specie</i>
<b>C 1s A</b>	284.80	284.80	284.80	C-C/C-H
<b>C 1s B</b>	<i>N.D.</i>	286.20	286.20	-COO <sup>-</sup> [7]
<b>C 1s B</b>	287.26	287.26	287.26	C-OH/C-O-C <sup>[7]</sup>
<b>W 4f<sub>5/2</sub></b>	37.83	37.57	37.83	Monoclinic (6+) <sup>[4a]</sup>
<b>W 4f<sub>7/2</sub></b>	35.67	35.46	35.67	Monoclinic (6+) <sup>[4a]</sup>
<b>O 1s A</b>	530.41	530.41	530.20	Lattice Oxygen <sup>[4a]</sup>
<b>O 1s B</b>	532.22	532.04	532.10	W-OH <sup>[8]</sup>
<b>N 1s A</b>	<i>N.D.</i>	399.98	399.98	-NH <sub>2</sub> /-NH- <sup>[8]</sup>
<b>N 1s b</b>	<i>N.D.</i>	401.71	401.71	NH <sub>4</sub> <sup>+</sup> [8]
<b>Cl 2p<sub>1/2</sub></b>	<i>N.D.</i>	199.51	199.51	Cl <sup>-</sup> [9]
<b>Cl 2p<sub>3/2</sub></b>	<i>N.D.</i>	197.97	197.97	Cl <sup>-</sup> [9]

**Table S3.** Fitted EIS results of photoanodes under simulated solar light irradiation based on the equivalent circuit.

<i>Photoanode</i>	<i>Rs/ohm</i>	<i>Rct/ohm</i>	<i>CPE/(F cm<sup>-2</sup>)</i>
<i>WO<sub>3</sub>-(PAH)<sub>4</sub></i>	<i>13.78</i>	<i>4931</i>	<i>0.0004062</i>
<i>WO<sub>3</sub></i>	<i>15.31</i>	<i>5416</i>	<i>0.0004105</i>
<i>WO<sub>3</sub>-(PAH)<sub>4</sub>-450 °C</i>	<i>15.87</i>	<i>6581</i>	<i>0.0002288</i>

**Note:**  $R_{ct}$  values were obtained by fitting the EIS results according to a simple equivalent circuit composed of a series of resistances (**Figure 3f**, inset).  $WO_3-(PAH)_4$  demonstrates the smallest  $R_{ct}$  in comparison with other counterparts under simulated solar light irradiation (AM 1.5G), indicative of its lowest interfacial charge transfer resistance.

**Table S4.** Fitted EIS results of photoanodes under visible light irradiation based on the equivalent circuit.

<i>Photoanode</i>	<i>Rs/ohm</i>	<i>Rct/ohm</i>	<i>CPE/(F cm<sup>-2</sup>)</i>
<i>WO<sub>3</sub>-(PAH)<sub>4</sub></i>	<i>17.37</i>	<i>2883</i>	<i>0.0007044</i>
<i>WO<sub>3</sub></i>	<i>13.55</i>	<i>4634</i>	<i>0.0003143</i>
<i>WO<sub>3</sub>-(PAH)<sub>4</sub>-450 °C</i>	<i>13.94</i>	<i>7332</i>	<i>0.0003715</i>

**Note:** WO<sub>3</sub>-(PAH)<sub>4</sub> demonstrates the smallest Rct in comparison with other counterparts under visible light irradiation ( $\lambda > 420$  nm), indicative of its lowest interfacial charge transfer resistance.

## References

- [1] J. Yang, W. Li, J. Li, D. Sun, Q. Chen, *J. Mater. Chem.* **2012**, 22, 17744.
- [2] B. Liu, E. S. Aydil, *J. Am. Chem. Soc.* **2009**, 131, 3985.
- [3] S. Kannan, N. P. Subiramaniam, S. U. Lavanisadevi, *J. Mater. Sci. Mater. Electron.* **2020**, 31, 8514.
- [4] a) Z. Zeng, T. Li, Y.-B. Li, X.-C. Dai, M.-H. Huang, Y. He, G. Xiao, F.-X. Xiao, *J. Mater. Chem. A* **2018**, 6, 24686; b) Q. Zhang, Q. An, X. Luan, H. Huang, X. Li, Z. Meng, W. Tong, X. Chen, P. K. Chu, Y. Zhang, *Nanoscale* **2015**, 7, 14002.
- [5] M.-H. Huang, Y.-B. Li, T. Li, X.-C. Dai, S. Hou, Y. He, G. Xiao, F.-X. Xiao, *Chem. Commun.* **2019**, 55, 10591.
- [6] R. R. Kharade, S. S. Mali, S. P. Patil, K. R. Patil, M. G. Gang, P. S. Patil, J. H. Kim, P. N. Bhosale, *Electrochim. Acta* **2013**, 102, 358.
- [7] F.-X. Xiao, Z. Zeng, B. Liu, *J. Am. Chem. Soc.* **2015**, 137, 13990.
- [8] C. Mo, J. Jian, J. Li, Z. Fang, Z. Zhao, Z. Yuan, M. Yang, Y. Zhang, L. Dai, D. Yu, *Energy Environ. Sci.* **2018**, 11, 3334.
- [9] S. Y. Yu, W. E. O. Grady, D. E. Ramaker, P. M. Natishan, *J. Electrochem. Soc.* **2000**, 147, 2952.